Boron isotope geochemistry of Na-bicarbonate, Na-chloride, and Ca-chloride waters from the Northern Apennine Foredeep basin: other pieces of the sedimentary basin puzzle

This is a preprint. Final version is subject to change. Cite as Authors (Year) Title. Geofluids, in press.
DOI: 10.1111/gfl.12124

Boron isotope geochemistry of Na-bicarbonate, Na-chloride and Ca-chloride waters from the Northern Apennine Foredeep basin: other pieces of the sedimentary basin puzzle

Tiziano Boschetti*, Lorenzo Toscani, Emma Salvioli Mariani

Department of Physics and Earth Sciences "Macedonio Melloni", University of Parma, Parco Area delle Scienze 157/A, 43124 Parma, Italy

*corresponding author: tiziano.boschetti@unipr.it

Abstract

The boron stable isotope ratio $\delta^{11}B$ of twelve water samples representative of three chemical facies (fresh Na-bicarbonate, brackish Na-chloride, saline and brine Ca-chloride) have been analyzed. Interpretation of the $\delta^{11}B$ along with the chemical composition reveals that Na-carbonate waters from the Northern Apennine are of meteoric origin, with boron contributions from clay-desorption and mixing with seawater-derived fluids of Na-chloride or Ca-chloride compositions. The comparison of our new results with the literature data on other sedimentary basins of Mediterranean and worldwide confirms the contribution of Na-bicarbonate waters to the genesis of mud volcano fluids. The Na-chloride sample of Salvarola (SAL), which may represent the end-member of the mud volcanoes, and the Ca-chloride brine water from Salsomaggiore (SM) indicate a boron release from clays compatible with the diagenetic process. The empirical equation:

$$\delta^{11}B = [5.1364 \times \ln(1/B)_{mg/l}] + 44.601$$

relating boron concentration and the stable isotope composition of the fluids observed in this study and the literature is proposed to trace the effect of diagenesis in sedimentary basins. A geothermometer associated to the diagenetic equation is also proposed:

$$T°C = [\delta^{11}B - 38.873 (\pm 1.180)] / [-0.164 (\pm 0.012)]$$

The application of this equation to obtain reservoir temperatures from $\delta^{11}B$ compositions of waters should be carefully evaluated against the results obtained from other chemical and isotopic geothermometers from other basins around the world..

Introduction

Sodium bicarbonate (Na-HCO_3) waters are found in coastal regions, coalbed methane production sites and sedimentary basins. In the coastal and coalbed sites, the chemical compositions of these waters have been mainly related to a Ca-for-Na exchange between water and clays (Appelo and Postma 2007; Committee on Management and Effects of Coalbed Methane Development and Produced Water in the Western United States et al. 2010), whereas in sedimentary basins, silicate hydrolysis and calcite precipitation have also been proposed (Toran and Saunders 1999; Venturelli et al. 2003). Since the 1950s, Na-HCO_3 waters from sedimentary basins have been considered a shallow indicator of the presence of hydrocarbons at depth (Kartsev et al. 1959; Collins 1975; Chilingar et al. 2003). The CO_2 produced by fermentation and anaerobic oxidation reactions occurring in conjunction with methanogenesis can be responsible for the high bicarbonate content in these waters (Grossman et al. 1989). Moreover, sedimentary basin Na-HCO_3 waters show other noteworthy features (Boschetti 2011), such as i) an unexpected high boron content (0.3 – 6 mg/l) in spite of their fresh salinity and ii) a manifest contribution to terrestrial mud volcano fluids. These important features notwithstanding, the boron isotope characterization of these waters is still

lacking. To address this gap, we investigated the physico-chemical parameters and both the concentrations and isotope compositions of boron in the Na-HCO_3 waters of the Northern Apennine Foredeep basin (NAF). Moreover, to better characterize the boron geochemistry of Na-HCO_3 waters and clarify their relationship with other typical waters of sedimentary basins, we investigated the boron stable isotopes of the NAF Ca-chloride (Ca-Cl) and Na-chloride (Na-Cl) waters from Boschetti et al. (2011). Using a global $\delta^{11}B$ versus 1/B diagram, the new data were compared with those from the literature on the formation brines, mud volcanoes, and offshore porewaters from both the Mediterranean area and worldwide. The way of grouping of the samples in the diagram helps to trace the effects of evaporation and adsorption-desorption from clays or other minerals that can change the boron geochemistry of the waters in sedimentary basins (Vengosh et al. 1992; Vengosh et al. 2000). The same approach was used to develop an empirical equation for diagenesis and a related graphical temperature-scale applicable to the waters. The still high uncertainty on the theoretical boric-borate (Zeebe 2005) and silica-water (Deyhle and Kopf 2005) fractionation factors makes suitable our empirical evaluations.

Geological settings

The Northern Apennines are a fold and thrust belt characterized by the stacking of several structural units of oceanic and continental origin (Fig. 1; e.g., Castellarin 2001). The complex structure of the chain is the result of the convergence and collision between the European and Adria plates from the Mesozoic to the present. The complete closure of the Piedmont–Ligurian Ocean (a portion of the Tethys) during the Middle–Late Eocene caused the rapid uplift and erosion of the Alpine orogenic wedge and the inception of continental collision. During collision (Late Oligocene to Recent), the internal oceanic units (Ligurian units) were forced over the western continental margin of Adria, and the thrust system migrated toward the foreland that included the Tuscan and Umbrian units, which were deposited on the Adria plate. Foredeep basins developed and migrated toward east and

northeast in response to the advancing Apenninic fronts, which progressively accreted the foredeep deposits. Currently, the Po Plain separates the foothills of the Northern Apennines to the south and the Southern Alps to the North (Fig. 1). A brief description of the lithology of the sampling sites is presented here to aid in understanding the geochemical features of the investigated waters.

Fresh Na-HCO_3 waters: The F3 and F6 spring waters issued from the marly to pelitic Mt. Caio flysch (Late Cretaceous), whereas the remaining three issued from sandstones: F8 and F10 spring from the Bismantova Formation (Late Priabonian-Late Rupelian) and F13 from the Ranzano Formation (Late Burdigalian (?)-Serravalian) (Toscani et al. 2001; Venturelli et al. 2003).

Brackish Na-Cl waters: The Miano (MI) water was sampled from a hydrocarbon research well drilled at Miano in the Municipality of Corniglio (Parma Province) near the Northern Apennine watershed (Fig. 1). The aquifer is composed of sandstones and clays of the Pracchiola Formation (at a depth of 850 to 1047 m; Heinicke et al. 2010). The Salvarola (SAL) water comes from a spa thermal bath in the Municipality of Sassuolo (Modena Province). The area is characterized by the emissions of fluids from mud volcanoes, so much so that it is assumed that the decreased activity of that outlets can be partly explained by the exploitation of subsurface fluids by the nearby Salvarola thermal plant (Bonini 2009).

The fluid reservoir of the local mud volcanoes is located at a depth of approximately 2 km (Bonini 2008), where the Marnoso-Arenacea Formation (turbiditic sandstones and siltstones, Early-Late Miocene) is overlain by the Ligurian units (dominant shales variably alternating with limestone layers, Jurassic-Oligocene). The pressurized fluids move up through discontinuities in the Ligurian Unit and accumulate in shallower reservoirs controlled by the lithological boundary between the impermeable claystones (Argille Azzurre Formation, Pliocene-Pleistocene) and the more permeable underlying deposits (Epi-Ligurian Units).

Saline and brine Ca-Cl waters: The samples were obtained from the Emilia-Romagna (from west to east: Salsomaggiore, SM; Monticelli, MON; Castelsanpietro, CSP; Fratta FRA) and Marche

(Tolentino, TOL) sectors of the NAF (Fig. 1), where the waters issue from hydrocarbon research wells and have been exploited for use as thermal spa baths. The strontium isotopes of the SM brine are marked by the lithology of the aquifer, in which the Burdigalian-Serravallian turbiditic deposits onlap Langhian hemipelagic marls (Conti et al. 2007; Boschetti et al. 2011). Other saline and brine waters are trapped within Miocene to Plio-Pleistocene clastic deposits, mostly turbidite sandstones, marine sands and mudstones (Veggiani 1964; Nanni and Vivalda 1999; Castellarin 2001; Capozzi and Picotti 2010).

Analytical methods

The five samples of fresh Na-HCO_3 (F3, F6, F8, F10, and F13) and the Na-Cl brackish water MI were sampled during April-May 2012. A complete description of the field and physico-chemical laboratory procedures is provided in Boschetti et al. (2011); therefore, these procedures are only briefly described here. The temperature, pH, redox potential (Eh), conductivity, total reduced N (as NH_4) and total reduced S (as H_2S) of the waters were measured in the field. In the laboratory, the total alkalinity (as HCO_3) was measured by Gran titration, whereas the major and trace elements of the waters (including boron) were determined by atomic emission and mass spectrometry inductively coupled plasma methods (ICP-AES and ICP-MS, respectively). The reported silica and chloride concentrations are the average of the results obtained by photometric-turbidimetric and ICP methods.

For fresh to brackish waters, the speciation of dissolved boron was calculated by averaging the results obtained by Debye-Hückel and Specific Ion interaction Theory (SIT) calculations, both using PHREEQCI version 3 software (Parkhurst and Appelo 2013). For the boron speciation in saline to brine waters, we averaged the results obtained from the extended Debye-Hückel (B-DOT) and Pitzer approaches, the former by EQ3/6 version 8 software (Wolery and Jarek 2003) and the latter by PHREEQCI.

The oxygen and hydrogen stable isotope composition of the water molecule was analyzed using the water–gas equilibration method. Briefly, water samples were transferred to a Finnigan GLF 1086 automatic equilibration device, online with a Finnigan DELTA-plus mass spectrometer (Laboratorio di Geochimica Isotopica at the University of Parma, Italy). The ratio measurements $^{2}H/^{1}H$ were obtained on pure hydrogen after the $H_2(g)$–$H_2O(l)$ equilibration using a catalyzer (Boschetti et al. 2005), whereas $^{18}O/^{16}O$ was measured on carbon dioxide after $CO_2(g)$–$H_2O(l)$ equilibration (Epstein and Mayeda 1953), both at 18 °C. Both ratios results were recorded in delta per mil (δ ‰) relative to the V-SMOW (Vienna Standard Mean Ocean Water) standard, thus obtaining the $\delta^{18}O$ and $\delta^{2}H$ values. The analytical precision was within ± 0.2 ‰ for oxygen and ± 1 ‰ for hydrogen.

The stable isotope composition of dissolved boron was measured both on the newly collected samples and on the six brackish to brine samples (SAL, CSP, FRA, TOL, MON, SM) previously collected and investigated by Boschetti et al. (2011). Aliquots of 0.45-μm-filtered water samples were stocked in PE bottles that were prewashed with 0.1 N Suprapur® HNO_3 (Merck Millipore) and rinsed with 18 Mohm water. The analysis was performed by multi-collector inductively coupled plasma mass spectrometry (MC-ICP-MS) and by negative thermal ionization mass spectrometry (N-TIMS) methods for the analysis of the fresh Na-HCO_3 and for the brackish to brine waters, respectively. Despite the different methods, the results are comparable according to the literature (Gonfiantini et al. 2003). The repeatability of the MC-ICP-MS procedure exhibited a standard deviation (2σ) better than 0.5‰, and the repeatability of the N-TIMS procedure exhibited a standard deviation (2σ) better than 0.7‰.

The boron stable isotope ratios are expressed in per mil (‰) δ-notation as follows:

$$\delta^{11}B\ (‰) = \frac{\left(^{11}B/^{10}B\right)_{sample} - \left(^{11}B/^{10}B\right)_{standard}}{\left(^{11}B/^{10}B\right)_{standard}} \times 10^{3}$$

This equation yields results expressed as the relative difference between the boron isotopic ratio of a sample and the boron acid SRM951 (National Bureau of Standards, Standard Reference Material No. 951) used as a standard.

Results

The main physico-chemical data and the stable isotope ratio composition of the water molecule and dissolved boron obtained in this study are reported in Table 1. The results are presented along with boron speciation by thermodynamic software (Appendix01) and the main characteristics discovered in previous studies as summarized in Figure 2.

The five Na-HCO_3 samples in this study exhibited B concentrations from 0.77 to 3.9 mg/l, distinctly enriched if compared with the local Ca-HCO_3 fresh groundwaters (Fig. 2A), and $\delta^{11}B$ from +6.1‰ to + 27.2‰. The Na-HCO_3 samples from the NAF are cold waters of meteoric origin (Fig. 2B) and are characterized by pH > 9, calcite oversaturation, fresh salinity and a positive relationship between the boron and chloride concentrations (Venturelli et al. 2003; Boschetti 2011). Generally, the temperature-controlled fractionation of B isotopes in aqueous solutions occurs between boric acid molecule [$B(OH)_3^\circ$ - trigonal] and borate complexes [$B(OH)_4^-$ - tetrahedral]. At 25°C, ^{11}B is preferentially partitioned into the boric acid whereas ^{10}B into the borates (Palmer and Swihart 1996). Moreover, boric acid and borates are dominant in solutions at pH < 9 and pH > 9, respectively. Despite their pH > 9 and calcite oversaturation, no $\delta^{11}B$ increase or B content decrease relations (due to ^{10}B adsorption) were found in our Na-HCO_3 samples. Moreover, thermodynamic speciation revealed a prevalence of borates (65%) only in F3, a prevalence of boric acid in F13 (76%) and an equal percentage of both in the F6, F8 and F10 springs (Appendix01). However, the unusually low pH of F13 (8.74) coupled with an excess of boric acid may be due to an excess of meteoric water. In fact, the pH and boron speciation of the 1998 data (Toscani et al. 2001) reveals

characteristics similar to F6, F8 and F10, i.e., pH = 9.22 and almost equal fractions of boric acid and borates (Appendix01).

The brine waters of the NAF have a Ca-Cl composition typical of the brines from sedimentary basins (Boschetti 2011; Boschetti et al. 2011). Previous chemical and isotope data reveled that these waters originated from the subaerial evaporation of Messinian seawater, beyond the point of gypsum precipitation but before halite precipitation, followed by dolomitization, albitization/zeolitization and illitization reactions during diagenesis (Fig. 2; Boschetti et al. 2011; Boschetti et al. 2013b). The brine samples of Tolentino (TOL; B = 8.2 mg/l, $\delta^{11}B$ = +37.9‰), Monticelli (MON; B = 18 mg/l, $\delta^{11}B$ = +35.1‰) and Salsomaggiore (SM; B = 358 mg/l, $\delta^{11}B$ = +13.2‰) exhibit a similar prevalence of boric acid (96-99%; Appendix01). The lower content and the slight ^{11}B enrichment of TOL could be due to B-uptake by clays (Fig. 2A). Differently, the saltiest SM brine has a much higher boron content and a lower boron isotope ratio. This peculiar characteristic of SM brine is most likely related to the diagenetic reactions that occurred in a closed-system environment at a maximum temperature of T = 157 ± 10 °C, as estimated by chemical and isotope geothermometers (Boschetti et al. 2011; Boschetti 2013) and according to the thermal evolution of the hydrocarbons (Capozzi and Picotti 2010), which led the SM waters to become ^{18}O enriched (up to $\delta^{18}O$ = +11.3‰) relative to the other formation brines from NAF (Fig. 2B). However, the boron speciation in SM is unaffected by the calculation at deep conditions (T = 157°C, P = 650 bar; Appendix01).

The two saline waters from the Romagna sector of the NAF (eastward of Bologna, Fig. 1) feature the following values: $\delta^{11}B$ = +26.6‰, B = 7.5 mg/l (CSP, Castelsanpietro) and $\delta^{11}B$ = +22.9‰, B = 12 mg/l (FR, Fratta). It is noteworthy that in these waters, the boron speciation is similar (93-99%) and the boron isotope composition is almost the average of the brine values described above, whereas the boron content is much lower. This pattern may occur because these saline waters

maintained the Ca-Cl characteristic of the brines but were diluted by more recent additions of meteoric or marine water (Fig. 2; Boschetti 2011; Boschetti et al. 2011).

The third group of samples involves the brackish Na-chloride waters. These waters show similar boron speciation but quite different total boron concentrations: $\delta^{11}B$ = +18.9‰, B = 100 mg/l, $B(OH)_3^\circ$ = 84% (SAL, Salvarola) and $\delta^{11}B$ = +14.0‰, B = 11 mg/l, $B(OH)_3^\circ$ = 89% (MI, Miano). These waters have additional interesting peculiarities. The chemical compositions of the SAL samples are related to the overpressured end-member of the mud volcanoes, which is not limited to the NAF but applicable to sedimentary basins worldwide (Fig. 2A; Boschetti 2011). The MI sample is a hot water sample (39°C) with dissolved thermogenic methane (Heinicke et al. 2010), probably originated by the mixing between meteoric water (Na-HCO_3 ?) and an overpressured Na-Cl or a saline-brine Ca-Cl water (Fig. 2).

Discussion

Preliminary discrimination between natural and anthropogenic boron sources

In Fig. 3A, the $\delta^{11}B$ and pH data of the samples are plotted along with the typical variation of seawater (Hemming and Hanson, 1992) and a local hypothetical groundwater with initial $\delta^{11}B$ = +10‰ (Boschetti et al. 2013a) used as terms of comparison. As expected, the Na-HCO_3 waters are distributed between the boric-borate extremes of the groundwater, confirming their meteoric origin, whereas saline and brine waters are plotted within the values of seawater. Exceptions are represented by the SM brine and the brackish waters (SAL, MI) which confirm the occurrence of more complexes processes during their origin (e.g. diagenesis, mixing).

To better understand the other possible sources of boron, the sampled waters have been plotted in the $\delta^{11}B$ versus B/Cl diagram (Fig. 3B). The different chemical facies are well distinguished by discrete B/Cl values. Similarly to other fresh bicarbonate springs from the Northern Apennine (Boschetti et al. 2013a), the Na-HCO_3 show high B/Cl values probably due to an uncontaminated

origin as testified by the clustering very close to (F6 sample) or above the hydrothermal fluids field (Fig. 3B). At the opposite side of the diagram, that is at quite lower B/Cl values, two brine (MON and TOL) plot near the present-day seawater, confirming their natural marine origin. The saline waters (CSP and FRA) show similar B/Cl ratios which, combined with lower $\delta^{11}B$ values, generate a trend toward possible contamination sources (fertilizers, sewages). However, this interpretation must be excluded because the saline and brine waters of this study are used for therapeutic purposes in the local spa thermal baths, where their safety is guaranteed by strict sanitary controls. Also at Salsomaggiore (SM) this type of contamination is not realistic because the aquifer circuit of the brine is closed to recent meteoric recharge (Boschetti et al. 2011), therefore its position on the boundary of seawage field (Fig. 3B) is a mere coincidence. Generally speaking, a $\delta^{11}B$ distinction between 'marine brines' and 'non-marine brines' was made by Vengosh et al. (1992): these authors proposed for 'marine brines' a range of $\delta^{11}B$ values between that of the Dead Sea ($\delta^{11}B$ = +57‰; Vengosh et al. 1991) and the present-day seawater ($\delta^{11}B$ = +39‰), whereas 0‰ < $\delta^{11}B$ < +39‰ for 'non-marine brines'. However, considering the $\delta^{11}B$ of our SM brine sample ($\delta^{11}B$ = +13.4‰;) and the lower value of $\delta^{11}B$ measured in the clastic-reservoir brines of the Gulf Coast ($\delta^{11}B$ = +10‰; Land, 1995; Williams et al., 2001c), it is evident that also seawater-derived formation brines modified by diagenetic processes may fall in the 'non-marine' field of Vengosh et al. (1992). Therefore, the formation brine field previously proposed in Boschetti et al. (2013) has been extended down to $\delta^{11}B$ = +10‰ according to the 'deep brines' field of Tonarini et al. (2009) and to the lower B/Cl values determined in this work (Fig. 3B).

Also for brackish samples SAL and MI, which plot between SM brine and the more ^{11}B-enriched Na-HCO_3 waters (Fig. 3B), the anthropogenic contamination can be excluded and other natural sources should be invoked for boron. In their original version of the $\delta^{11}B$ versus B/Cl diagram, Vengosh et al. (1998b) do not report the field of the boron contribution from clays. Probably this was due to the lack of an extended clay dataset at that time, and/or to the lack of chloride data

associated to the boron concentration and $\delta^{11}B$ value of the clays. At present, it is assumed that clay desorption effect in the offshore porewaters occurs with no chloride release (e.g. Chao and You 2006). Therefore, as first approximation, the concentration of the desorbed boron from clays measured by Spivack et al. (1987) has been divided by the chloride content of the present-day seawater, in this way defining the "porewater" field of Fig. 3B.

The MI, SM and F8 samples fall within the $\delta^{11}B$ range of clay desorption, but with higher B/Cl respect to the expected porewater field. For brackish (MI) and fresh (F8) waters this may be due to the increasing contribution of meteoric water, whereas in SM brine many effects may have influenced its composition as i) several cycles of seawater evaporation-seawater ingression-meteoric dilution during Messinian (Boschetti et al. 2011), and ii) the temperature of diagenesis up to 157°C (Boschetti et al. 2011; Boschetti 2013). According to Williams et al. (2001b,c), during burial from surface to the diagenesis-methamorphism boundary, the boron contribution from clay may have switched from a desorption/interlayer to a crystal lattice source, and the clay mineralogy of the aquifer may be evolved from smectite to illite. The extreme $\delta^{11}B$ values of the boron from smectite and illite crystal lattice may be assumed to be +10‰ and -10‰, respectively, with no difference between clays of terrestrial or marine origin (Ishikawa and Nakamura 1993, Williams et al. 2001c). Mixed layer clays shift between the above $\delta^{11}B$ extreme values (Williams et al. 2001b,c; Williams and Hervig, 2002). Also for crystal lattice clays, is difficult to give a discrete B/Cl value due to the lack of chloride concentration data. Gurenko and Kamenetsky (2011) gave the values B = 11.1 mol and Cl = 28.2 mol (B/Cl = 3.94×10^{-1}) for the siliceous (illitic) sediments, but the Cl content was assumed in an arbitrary way. Therefore, it could be a mere coincidence that SM brine and MI brackish waters fall on the mixing line between the (illitic) sediment field and seawater.

Discrimination between natural sources and fractionation effects

Since the $\delta^{11}B$ versus B/Cl diagram does not give an exhaustive explanation of the boron sources, the samples have been plotted also in the $\delta^{11}B$ versus 1/B diagram (Fig. 4). There, the sedimentary basin Na-HCO_3 waters are grouped on the side of the waters of meteoric origin but are shifted toward the seawater-meteoric divide relative to the coalbed Na-HCO_3 waters (Vinson et al. 2013). The boron isotope geochemistry of both Na-HCO_3 groups can most likely be explained by the mixing of two or three end-members (Fig. 4): rainwater (Millot et al. 2010) and the B-desorption from clays (Spivack et al. 1987) for the coalbed Na-HCO_3 waters, and these two end-members with the addition of a seawater end-member form the sedimentary basin Na-HCO_3 waters. In fact, the high B and Cl contents and the water isotope composition of the water issued from F10 spring have previously been explained as the mixing of meteoric waters and a seawater-derived formation brine (Toscani et al. 2001; Boschetti 2011). Further distinction between the two groups of Na-HCO_3 waters is given by the composition of methane; in fact, if coalbed Na-HCO_3 waters contain methane of exclusively microbial origin (Vinson et al. 2013), the Na-HCO_3 waters from the sedimentary basin show separate associations of high $\delta^{11}B$ values with microbial methane (F3, F6, and F10) and low $\delta^{11}B$ with thermogenic methane (F6, Fig. 4; Lorenzi 2013). This latter association may indicate the contribution of a deeper source of hydrocarbons and boron (basement groundwaters in Fig. 4). It is also noteworthy that both the data from Verrua (Monferrato, Italy, Alpine orogeny), a fossil mud volcano whose composition was obtained by the authigenic carbonates (Kopf and Deyhle 2002), and the lower 1/B-$\delta^{11}B$ values obtained by a preliminary screening of the mud volcano fluids from the NAF (Pennisi et al. 2013) plot near our Na-HCO_3 field (Fig. 4). This finding confirms that sedimentary Na-HCO_3 waters take part in the genesis of the mud volcano's fluids (Boschetti 2011).

On the "seawater side" of the $\delta^{11}B$-1/B diagram (Fig. 4), the TOL and MON brines plot near the evaporation curve starting from the present-day value of the Mediterranean Sea, $\delta^{11}B$ = +37.7‰ (Vengosh et al., 1992). This finding supports the origin of these waters described in Boschetti et al. (2011). Moreover, the slight shift down the evaporation path is more consistent with an evaporation

starting during the Messinian Salinity Crisis. The Messinian values of $\delta^{11}B = +34.6 \pm 1.6‰$ and B = 6.45 ± 0.23 mg/l were obtained using the porewaters from Messinian strata of the Deep Sea Drilling Project "site 372" from the Provence basin in the western Mediterranean (Vengosh et al., 2000). These values are consistent with the slightly lower $\delta^{11}B$ (approximately 2‰) of Messinian seawater in comparison with modern seawater (Lemarchand et al. 2002).

The CSP and FRA saline waters show lower $\delta^{11}B$ and fall between the seawater and the B-desorption field (Fig. 4), which is occupied by the MI brackish water.

The SM brine and SAL brackish waters deserve special attention. In Fig. 4, the line connecting the SM and SAL samples with seawater and the seawater evaporation line delimit a triangular area within which some of the Mediterranean porewaters fall. According to Vengosh et al. (2000), other porewaters were affected by boron adsorption on minerals, particularly for the samples clustered above the line representing the evaporation of their seawater component (Fig. 4). In contrast, the porewaters shifted down the evaporation line and grouped near the line joining the SAL and SM samples with seawater, might represent diagenetic boron from clay minerals following stress-driven or temperature-induced effects, as described by Deyhle et al. (2003). In fact, both the B concentration (105 mg/l) and $\delta^{11}B$ (+18.9‰) of the overpressured SAL sample resemble those estimated for the fluid issuing from the mud volcano of the site 808-Nankai Trough, which is originated in the proximity of the decollement zone ($B \cong 108$ mg/l and $\delta^{11}B \cong +20‰$; You et al. 1996). In contrast, the SM brine experienced water-rock diagenetic reactions at a peak temperature of 157°C. For further proof that the boron in the SAL and SM samples is derived from the interaction of the waters with clays, it should be noted that the lines fit to these samples point toward the 'mud and mudstones' field (Fig. 4). This latter field, deduced by various data from the literature (Spivack et al. 1987; Kopf and Deyhle 2002; Lavrushin et al. 2003; Mata et al. 2012), has values of $\delta^{11}B$ from -10‰ to +10‰ according to the previous estimation of clay composition (Ishikawa and Nakamura 1993, Williams et al. 2001c). It could be argued that, in addition to

illitization, the SM brine also underwent dolomitization and albitization-zeolitization and that the boron effect due to the interaction with these minerals was never investigated. Using the silicate-water fractionation equation for boron of Williams et al. (2007), $\delta^{11}B_{fluid}$ = +13.2‰ and the temperature T = 157°C estimated for SM, a $\delta^{11}B_{mineral}$ = -7.6‰ was found, which corresponds to the lower area of the mud and mudstone field of Fig. 3, and to an illitic-tetrahedral boron (Williams et al. 2007). However, a contribution of kerogen to the high B concentration (approximately 1000 mg/kg) and lower $\delta^{11}B$ value of this field cannot be excluded (Harder 1973; Williams et al. 2001a; Środoń and Paszkowski 2011).

The $\delta^{11}B$-B diagenetic equation and a possible temperature key

In Fig. 5, we compare the samples of the present study with sedimentary brines and mud volcano waters from several sites outside of the Mediterranean basin. It is noteworthy that some mud volcano samples showing diluted salinities and/or sampled in terrestrial sites are shifted toward the sedimentary basin Na-HCO_3 field of the present study (Fig. 5). Sedimentary brines from the Gulf Coast (Land and Macpherson 1992; Moldovanyi et al. 1994; Land 1995) and France (Millot et al. 2011) are within the seawater-diagenetic triangle previously described. As expected, the brines from siliciclastic aquifers of the Gulf Coast and France are scattered near the diagenetic curve, distinct from those from carbonate aquifers of the Gulf Coast. The high scattering exhibited by the Gulf Coast brines from siliciclastic aquifers may be due to several effects, such as clay-desorbed boron and mixing with cold, recent seawater or freshwater (Land and Macpherson 1992; Land 1995). However, the median values of all the siliciclastic Gulf Coast brines, B = 76 mg/l (1/B = 0.013) and $\delta^{11}B$ = +21‰, fall very close to the diagenetic line. Based on our data and from those previously reported data, we obtain the following best fit (Fig. 6A; Appendix02a):

$$\delta^{11}B = [5.1364 \times \ln(1/B)_{mg/l}] + 44.601$$

We suppose that this equation may represent the relation between dissolved boron and its isotopic composition due to diagenetic effect in the sedimentary basins. The logarithmic equation was chosen because it is the expected fit for samples affected by fractionation (as evaporation and adsorption effects reported in Fig. 4 and Fig. 5). Since tests of statistical significance in nonlinear regression are often meaningless and misguided (McFadden 2001), the robustness of the logarithmic equation was checked by two PC programs which compare and rank every possible fit by using standard errors and regression coefficients, and finally report the best one (Curve Expert Basic 1.4 – Hyams, 2010; TableCurve2D, Systat Software, San Jose, CA). Both PC programs confirm that the logarithmic equation is the best model for fitting the data.

In Fig. 6B, we tentatively propose a tentative temperature scale related to the diagenetic equation. The distribution of the $\delta^{11}B$ and temperature data of the samples data is compared with two curves showing the evolution of the water composition after interaction with clays (both smectitic and illitic) and calculated by the Rayleigh fractionation model (Clark and Fritz 1997; Rosner et al. 2003):

$$\delta^{11}B_{water} = \left[\left(\delta^{11}B_{in.clay} + 10^3 \right) \cdot \alpha_{water\text{-}clay} \cdot f^{\left(\alpha_{water\text{-}clay} - 1 \right)} \right] - 10^3$$

$\delta^{11}B_{in.clay}$ represents the initial value of an hypothetical smectitic ($\delta^{11}B_{in.clay}$ = +5 ‰) and illitic ($\delta^{11}B_{in.clay}$ = -5 ‰) clays, respectively (Fig. 2, Fig 3); $\alpha_{water\text{-}clay}$ the fractionation factor of Williams et al. (2001b); *f* is the fraction of boron in the clay ($f = B_{t>0} / B_{t=0}$, where $B_{t=0}$ is the boron content at the beginning of the interaction), which is assumed to be a linear function of temperature (Rosner et al. 2003). The reservoir temperature or the temperature measured at depth of the samples shown in Fig.6A have been projected in Fig.6B. Concerning the site 372 porewaters in the Messinian stratum,

the measured temperature values were between 24-28°C (Erickson and Von Herzen 2007) and their shift to low $\delta^{11}B$ is compatible with the presence of illite in the sediments (Chamley et al. 2007). The mean temperatures determined by chemical and/or isotope geothermometers have been reported for French (Millot et al. 2011), Gulf Coast (Land and MacPherson 1992, Williams et al. 2001c) and our SM brine samples (Boschetti 2013; Boschetti et al. 2011). The evaluation of the temperature for stress-affected waters as site 808-Nankai Trough and SAL mud volcanoes deserves a separate discussion, because the pressure-induced effect on boron fractionation may be greater than the temperature effect. The supposed temperature at the decollement zone of site 808-Nankai Trough was about 100-120 °C (Moore et al. 2005, You et al. 1993). This corresponds and agrees with the temperature range estimated by the gas composition of the Apennine mud volcanoes (Tassi et al. 2012), which are represented by SAL sample in Fig. 6B. It is noteworthy that the linear best fit of the $\delta^{11}B$-temperature data of the samples included in the diagenetic equation is the diagonal between the two curves representing the water-clay interaction modeling. Finally, from this latter linear regression (Appendix02b), the following geothermometric equation for diagenetic process has been obtained:

$$T°C = [\delta^{11}B - 38.873 (\pm 1.180)] / [-0.164 (\pm 0.012)]$$

Conclusions

The examination of the boron concentrations and boron stable isotope ratios of three geochemical water facies from the Northern Apennine Foredeep basin revealed interesting characteristics. The fresh Na-HCO_3 waters featured $\delta^{11}B$ values of between +6.1‰ and +27.2‰ associated with high boron contents of between 0.77 mg/l and 3.9 mg/l. The origin of boron in these waters can be explained by mixing of three component as meteoric water, seawater (or a seawater-derived formation brine) and B-desorption from clays. In Na-HCO_3 waters, the contribution of another B component (with low $\delta^{11}B$) and thermogenic hydrocarbon from a deeper source cannot be excluded,

but it should be confirmed by a systematic sampling campaign in the area. However, the role of Na-HCO_3 waters in the genesis of the mud volcanoes is confirmed. The seawater-derived origin of the Ca-Cl saline and brine waters from the NAF is also confirmed, but the diagenetic reactions that involve clays (and kerogen) may lower the $\delta^{11}B$ value and increase the concentration of the dissolved boron. The comparison of the concentration of boron and the $\delta^{11}B$ values of several Ca-Cl formation brines and Na-HCO_3 waters from porewaters and mud volcanoes (from the Mediterranean area and other sites worldwide) has permitted to find an equation and an associated temperature scale that describes the diagenetic effect and that can be used to characterize this process in the fluids from sedimentary basins. The obtained $\delta^{11}B$-T geothermometer has a great potential advantage because it permits to determine the temperature by knowing only the $\delta^{11}B$ value of the fluid, whereas the clay-water fractionation factors necessitate of the $\delta^{11}B$ value of the interacting clay. However, its utilization must be preceded by the verification of the position of the water sample in the $\delta^{11}B$-1/B diagram, that is on the diagenetic line. Therefore, considering that its direct application should be carefully evaluated, we suggest to use the $\delta^{11}B$-T equation in combination with classical chemical and isotopic geothermometers.

Acknowledgements

We would like to thank the two anonymous reviewers for their insightful suggestions and comments.

Table and Figure captions

Table 1 – Physico-chemical data and $\delta^{2}H(H_2O)$, $\delta^{18}O(H_2O)$, $\delta^{11}B$ isotope composition of the samples. Physico-chemical and water isotope data of the SAL, CSP, FRA, MON, TOL, and SM

samples are from Boschetti et al. (2011). Boron in mg/kg is calculated as follows: $[B]_{mg/kg} = [B]_{mg/l} / [density]_{kg/l}$.

Figure 1 - Simplified geological map of the Northern Apennines (after Boschetti et al. 2013). Codes in parentheses refer to the water samples analyzed in this study. The dotted field depicts the area where Na-HCO_3 waters were sampled. In the inset, *E-R*: Emilia-Romagna region; *M*: Marche region.

Figure 2 - B vs. Cl (A) and water isotope (B) diagrams of the waters from the Northern Apennine, modified from Boschetti (2011) and Boschetti et al. (2011), respectively. Green field: groundwater of meteoric origin. Pink field: overpressured waters (mud volcanoes were updated with the data from Oppo et al. 2013). Brown field: diagenetic water (Boschetti et al., 2011). Blue tones: Ca-Cl waters. In (A): *g* and *h* are the points of gypsum and halite saturation during seawater evaporation, respectively; dashed lines represent binary mixing. In (B): GMWL (Rozanski et al. 1993), cimwl and nimwl (Longinelli and Selmo 2003) are global, Central Italy and Northern Italy meteoric water lines, respectively; dotted circles enclose both data variations from long-term analysis of the well fields and salt effect on isotope composition (isotope activity, Boschetti et al. 2011); Open pentagon: V-SMOW, Closed pentagon: Northern Adriatic sea (Boschetti et al. 2011).

Figure 3 - (A) $\delta^{11}B$ vs. pH of the sampled waters (see Appendix01 for dissolved B speciation) compared with isotopic variation of boric acid $B(OH)_3^{\circ}$ and borate ion $B(OH)_4^-$ in seawater (Hemming and Hanson 1992) and with a hypothetical local groundwater with initial $\delta^{11}B = +10‰$ (Boschetti et al., 2013a). (B) $\delta^{11}B$ vs. B/Cl molar ratio values of sampled waters and potential boron sources (modified from Vengosh et al. 1998b and Boschetti et al. 2013a). The formation brine field of Boschetti et al. (2013a) has been extended according to the $\delta^{11}B$ values of the 'deep brine' field

of Tonarini et al. (2009) and the B/Cl of the brines from this study. Red square depicts the clay desorption effect in offshore porewaters (Chao and You 2006; Spivack et al. 1987), whereas red circle the hypothetical compositions of the (siliceous-illitic?) sediments (Gurenko and Kamenetsky 2011).

Figure 4 - $\delta^{11}B$ vs. 1/B (weight basis for solids and volume basis for fluids) diagram. The waters from the Northern Apennine Foredeep (NAF, this work, symbols as Fig. 3; extreme values of the mud volcano fluids are from Pennisi et al. 2013) are compared with other samples from Mediterranean sedimentary basins (literature): colored symbols and bricked field are porewaters (Vengosh et al. 1998a; Vengosh et al. 2000) and mud volcanoes (Kopf and Deyhle 2002; Deyhle et al. 2003), respectively (key). Note that the symbol dimension and logarithmic scale of the 1/B abscissa cancel the gap between weight and volume basis concentrations (see Table 1). The bold dashed line marks the limit between seawater (left side) and meteoric (right side) fields. The seawater data and evaporation effect line are from Vengosh et al. (1992), and the B-adsorption effect line is from Vengosh et al. (2000). The line representing the hypothetical diagenetic effect has been obtained in the present study. Rainwater (Millot et al. 2010), coalbed Na-HCO_3 waters (Vinson et al. 2013), basement groundwater (Barth 2000), clay desorption (Spivack et al. 1987), mud and mudstones (Spivack et al. 1987; Kopf and Deyhle 2002; Lavrushin et al. 2003; Mata et al. 2012) are represented as fields.

Figure 5 - $\delta^{11}B$ vs. 1/B (weight basis for solids and volume basis for fluids) diagram. The waters from the Northern Apennine Foredeep (this work; symbols as in Fig. 2) are compared with samples from sedimentary basins located out of Mediterranean (literature): formation brines from the Gulf Coast (Land and Macpherson 1992; Moldovanyi et al. 1994; Land 1995) and France (Millot et al. 2011) and mud volcano fluids from Taiwan (Chao et al. 2011), the Caucasus (Kopf et al. 2003;

Lavrushin et al. 2003), India (Kopf and Deyhle 2002) and China (Chunfang et al. 2006). The generalized fields, seawater data and B-fractionation paths (arrows) are the same as in Fig. 4. Dotted lines indicate mixing between two end-members.

Figure 6 – (A) Logarithmic best fit of the $\delta^{11}B$ and 1/B (volume basis) data of representative waters affected by diagenesis (data in Appendix02). *R* is the correlation coefficient and *S* the standard error (gray area) of the regression curve fit (equation). Literature data: site 372 porewaters from Messinian strata (Vengosh et al. 2000), formation brines from France (Millot et al. 2011), formation brines from the Gulf Coast (Land and Macpherson 1992; Land 1995), site 808-Nankai Trough mud volcano representative of the stress-induced B release (You et al. 1996) and present-day seawater (Vengosh et al. 1992). (B) $\delta^{11}B_{water}$-temperature scale diagram of the diagenetic equation. Samples have been projected using the temperature data measured at depth or estimated by classical chemical and/or isotopic geothermometers (see text for details and references). Curves: $\delta^{11}B_{water}$ evolution by the Rayleigh fractionation model supposing the interaction with a smectitic ($\delta^{11}B_{in.smectite}$ = +5‰) or illitic ($\delta^{11}B_{in.illite}$ = -5‰) clay (see text for details). Dashed line between the curves: best-fit of the samples. Hatched field: probable temperature range of stress-induced waters from mud volcanoes (SAL, site 808-Nankai Trough; see text for details).

References

Appelo CAJ & Postma D (2007) *Geochemistry, groundwater and pollution*, 2nd edn. The Netherlands, A.A. Balkema.

Barth SR (2000) Geochemical and boron, oxygen and hydrogen isotopic constraints on the origin of salinity in groundwaters from the crystalline basement of the Alpine Foreland. *Applied Geochemistry*, **15**,937-952.

Bonini M (2008) Elliptical mud volcano caldera as stress indicator in an active compressional setting (Nirano, Pede-Apennine margin, northern Italy). *Geology*, **36**,131–134.

Bonini M (2009) Mud volcano eruptions and earthquakes in the Northern Apennines and Sicily, Italy. *Tectonophysics*, **474**,723–735.

Boschetti T (2011) Application of Brine Differentiation and Langelier-Ludwig plots to fresh-to-brine waters from sedimentary basins: diagnostic potentials and limits. *Journal of Geochemical Exploration*, **108**,126-130.

Boschetti T (2013) Oxygen isotope equilibrium in sulfate-water systems: a revision of geothermometric applications in low-enthalpy systems. *Journal of Geochemical Exploration*, **124**,92-100.

Boschetti T, Etiope G, Pennisi M, Romain M & Toscani L (2013a) Boron, lithium and methane isotope composition of hyperalkaline waters (Northern Apennines, Italy): Terrestrial serpentinization or mixing with brine? Applied Geochemistry, 32,17–25.

Boschetti T, Manzi V & Toscani L (2013b) Messinian Ca–Cl Brines from Mediterranean Basins: Tracing Diagenetic Effects by Ca/Mg Versus Ca/Sr Diagram. *Aquatic Geochemistry*, **19**,195-208.

Boschetti T, Toscani L, Shouakar-Stash O, Iacumin P, Venturelli G, Mucchino C & Frape SK (2011) Salt waters of the Northern Apennine Foredeep Basin (Italy): origin and evolution. *Aquatic Geochemistry*, **17**,71–108.

Boschetti T, Venturelli G, Toscani L, Barbieri M, Mucchino C (2005) The Bagni di Lucca thermal waters (Tuscany, Italy): an example of Ca-SO_4 waters with high Na/Cl and low Ca/SO_4 ratios. *Journal of Hydrology*, **307**, 270-293.

Capozzi R & Picotti V (2010) Spontaneous fluid emissions in the Northern Apennines: geochemistry, structures and implications for the petroleum system. In: *Hydrocarbons in Contractional Belts. Geological Society Special Publications 348* (eds Goffey G, Craig J, Needham T & Scott R) London, The Geological Society of London, 115–135.

Castellarin A (2001) Alps-Apennines and Po Plain-Frontal Apennines Relationships. In: *Anatomy of an Orogen: the Apennines and Adjacent Mediterranean Basins* (eds Vai GB & Martini PI) Dordrecht, Springer Science+Business Media, 177-196.

Chamley H, de Segonzac GD & Mélières F (2007) 11.1 Clay Minerals in Messinian Sediments of the Mediterranean Sea. In, DSDP Volume XLII Part 1, 11. Special Mineralogical Studies, 389-395.

Chao HC & You CF (2006) Distribution of B, Cl and Their Isotopes in Pore Waters Separated from Gas Hydrate Potential Areas, Offshore Southwestern Taiwan. Terrestrial, Atmospheric and Oceanic Sciences, 17,961-979.

Chao HC, You CF, Wang BS, Chung CH & Huang KF (2011) Boron isotopic composition of mud volcano fluids: implications for fluid migration in shallow subduction zones. *Earth and Planetary Science Letters*, **305**,32–44.

Chilingar GV, Buryakovsky LA, Eremenko NA & Gorfunkel MV (2003) *Geology and geochemistry of oil and gas. Developments in Petroleum Science, Vol. 52*. Amsterdam, The Netherlands, Elsevier.

Chunfang C, Licai P, Bowen M & Yingkai X (2006) B, Sr, O and H isotopic compositions of formation waters from the Bachu Bulge in the Tarim Basin. *Acta Geologica Sinica*, **80**,550-556.

Clark IA & Fritz P (1997) *Environmental Isotopes in Hydrogeology*. Boca Raton, New York, Lewis Publishers-CRC Press.

Collins AG (1975) *Geochemistry of oilfield waters. Developments in Petroleum Science, Vol. 1*. Amsterdam, The Netherlands, Elsevier.

Committee on Management and Effects of Coalbed Methane Development and Produced Water in the Western United States, Committee on Earth Resources & National Research Council (2010) *Management and Effects of Coalbed Methane Produced Water in the Western United States*. Washington DC, National Academy of Sciences.

Conti A, Artoni A & Piola G (2007) Seep-carbonates in a thrust-related anticline at the leading edge of an orogenic wedge: The case of the middle–late Miocene Salsomaggiore Ridge (Northern Apennines, Italy). *Sedimentary Geology*, **199**,233–251.

Deyhle A & Kopf AJ (2005) The use and usefulness of boron isotopes in natural silicate–water systems. *Physics and Chemistry of the Earth*, **30**,1038–1046.

Deyhle A, Kopf AJ & Aloisi G (2003) Boron and boron isotopes as tracers for diagenetic reactions and depth of mobilization, using muds and authigenic carbonates from eastern Mediterranean mud volcanoes. In: *Subsurface Sediment Mobilization* (eds Van Rensbergen P, Hillis RR, Maltman AJ & Morley CK) London, The Geological Society, **216**, 491-503.

Epstein S, Mayeda T (1953) Variations of $^{18}O/^{16}O$ ratio in natural waters *Geochimica et Cosmochimica Acta*, **4**, 213–224.

Erickson AJ & Von Herzen RP (2007) 43. Down-Hole Temperature Measurements, Deep Sea Drilling Project, Leg 42A. In, DSDP Volume XLII Part 1, Section 6. Geophysical Studies, 857-871.

Gonfiantini R, Tonarini S, Adorni-Braccesi A, Al-Ammar AS, Astner M, Bächler S, Barnes RM, Bassett RL, Cocherie A, Deyhle A, Dini A, Ferrara G, Gaillardet J, Grimm J, Guerrot C, Krähenbühl U, Layne G, Lemarchand D, Meixner A, Northington DJ, Pennisi M, Reitznerová E, Rodushkin I, Sugiura N, Surberg R, Tonn S, Wiedenbeck M, Wunderli S, Xiao Y & Zack T (2003) Intercomparison of boron isotope and concentration measurements. Part II: evaluation of results. *Geostandards Newsletter*, **27**,41-57.

Grossman EL, Coffman BK, Fritz SJ & Wada H (1989) Bacterial production of methane and its influence on ground-water chemistry in east-central Texas aquifers. *Geology*, **17**,495-499.

Gurenko AA & Kamenetsky VS (2011) Boron isotopic composition of olivine-hosted melt inclusions from Gorgona komatiites, Colombia: New evidence supporting wet komatiite origin. *Earth and Planetary Science Letters*, **312**,201–212.

Harder H (1973) Boron. In: *Handbook of geochemistry* (ed. Wedepohl KH) Berlin, Springer-Verlag, B-O.

Heinicke J, Italiano F, Koch U, Martinelli G & Telesca L (2010) Anomalous fluid emission of a deep borehole in a seismically active area of Northern Apennines (Italy). *Applied Geochemistry*, **25**,555–571.

Hemming NG & Hanson GN (1992) Boron isotopic composition and concentration in modern marine carbonates. *Geochimica et Cosmochimica Acta*, **56**,537–543.

Hyams DG (2010) *CurveExpert Basic, Release 1.4*. http://docs.curveexpert.net/curveexpert/basic/_static/CurveExpertBasic.pdf

Ishikawa T & Nakamura E (1993) Boron isotope systematics of marine sediments. *Earth and Planetary Science Letters*, **117**,567-580.

Kartsev AA, Tabasararanskii ZA, Subbota MI & Mogilevskii GA (1959) *Geochemical Methods of Prospecting and Exploration for Petroleum and Natural Gas*. Berkeley and Los Angeles, University of California Press.

Kopf AJ & Deyhle A (2002) Back to the roots: boron geochemistry of mud volcanoes and its implications for mobilization depth and global B cycling. *Chemical Geology*,195– 210.

Kopf A, Deyhle A, Lavrushin VY, Polyak BG, Gieskes JM, Buachidze GI, Wallmann K & Eisenhauer A (2003) Isotopic evidence (He, B, C) for deep fluid and mud mobilization from mud volcanoes in the Caucasus continental collision zone. *International Journal of Earth Sciences*, **92**,407-425.

Land LS (1995) Na-Ca-Cl saline formation waters, Frio Formation (Oligocene), south Texas, USA: products of diagenesis. *Geochimica et Cosmochimica Acta*, **59**,2163-2174.

Land LS & Macpherson GL (1992) Origin of saline formation waters, Cenozoic section, Gulf of Mexico Sedimentary Basin. *American Association of Petroleum Geologists Bulletin*, **76**,1344–1362.

Lavrushin VY, Kopf A, Deyhle A & Stepanets MI (2003) Formation of mud-volcanic fluids in Taman (Russia) and Kakhetia (Georgia): evidence from boron isotopes. *Lithology and Mineral Resources*, **38**,120–153.

Lemarchand D, Gaillardet J, Lewin E & Allègre CJ (2002) Boron isotope systematics in large rivers: implications for the marine boron budget and paleo-pH reconstruction over the Cenozoic. *Chemical Geology*, **190**,123–140.

Longinelli A, Selmo E (2003) Isotopic composition of precipitation in Italy: a first overall map. *Journal of Hydrology*, **270**, 75–88.

Lorenzi F (2013) Caratterizzazione geochimica e geochimico-isotopica delle acque sodio bicarbonatiche dell'Appennino Settentrionale. In: *Department of Physics and Earth Sciences "Macedonio Melloni"* Parma, Italy, University of Parma, Master Degree Thesis.

Mata P, Williams LB, Nieto F, Martos R & Sáinz-Díaz CI (2012) Preliminary B and Li isotope data of illite/smectite from mud volcano sediments from the Gulf of Cádiz. *Macla*, **16**,100-101.

McFadden D (2001) On selecting regression variables to maximize their significance. In: *Nonlinear Statistical Modeling: Proceedings of the Thirteenth International Symposium in Economic Theory and Econometrics: Essays in Honor of Takeshi Amemiya* (eds Hsiao C, Morimune K, Powell JL), Cambridge University Press, Chapter 9, 259-280

Millot R, Guerrot C, Innocent C, Négrel P & Sanjuan B (2011) Chemical, multi-isotopic (Li–B–Sr–U–H–O) and thermal characterization of Triassic formation waters from the Paris Basin. *Chemical Geology*, **283**,226–241.

Millot R, Petelet-Giraud E, Guerrot C & Negrel P (2010) Multi-isotopic composition (δ^7Li–δ^{11}B–δD–δ^{18}O) of rainwaters in France: Origin and spatio-temporal characterization. *Applied Geochemistry*, **25**,1510–1524.

Moldovanyi EP, Walter LM & Land LS (1994) Strontium, boron, oxygen, and hydrogen isotope geochemistry of brines from basal strata of the Gulf Coast sedimentary basin, USA. *Geochimica et Cosmochimica Acta*, **57**,2083–2099.

Moore GF, Mikada H, Moore JC, Becker K & Taira A (2005) Legs 190 and 196 synthesis: deformation and fluid flow processes in the Nankai Trough accretionary prism. In: Proceedings of the Ocean Drilling Program, Scientific Results Volume 190/196 eds Mikada H, Moore GF, Taira A, Becker K, Moore JC & Klaus A), http://www-odp.tamu.edu/publications/190196SR/synth/synth.html.

Nanni T & Vivalda P (1999) Le acque salate dell'avanfossa marchigiana: origine, chimismo e caratteri strutturali delle zone di emergenza. *Bollettino della Societa Geologica Italiana*, **118**,191–215.

Oppo D, Capozzi R, Picotti V (2013) A new model of the petroleum system in the Northern Apennines, Italy. *Marine and Petroleum Geology*, **48**, 57–76

Palmer MR & Swihart GH (1996) Boron isotope geochemistry; an overview In: *Boron: Mineralogy, Petrology, and Geochemistry* (eds Grew ES & Anovitz LM) Washington D.C., Mineralogical Society of America, **33**, 709-744.

Parkhurst DL & Appelo CAJ (2013) Description of Input and Examples for PHREEQC Version 3 - A Computer Program for Speciation, Batch-Reaction, One-Dimensional Transport, and Inverse Geochemical Calculations. In, U.S. Geological Survey Techniques and Methods, **book 6, chap. A43**, 497.

Pennisi M, Battaglia S & Martinelli G (2013) Mineralogy and boron geochemistry of mud volcanoes from Northern Apennines (Italy). *Mineralogical Magazine*, **77**,1947.

Rosner M, Erzinger J, Franz G & Trumbull R (2003) Slab-derived boron isotope signatures in arc volcanic rocks from the Central Andes and evidence for boron isotope fractionation during progressive slab dehydration. *Geochemistry Geophysics Geosystems G3*, **4**,DOI: 10.1029/2002GC000438.

Rozanski K, Araguás-Araguás L, Gonfiantini R (1993) Isotopic patterns in modern global precipitation. In: *Climate Change in Continental Isotopic Records* (eds Swart PK, Lohmann KC, Mckenzie J, Savin S) Geophysical Monograph **78**. American Geophysical Union, Washington, D.C.

Spivack AJ, Palmer MR & Edmond JM (1987) The sedimentary cycle of the boron isotopes. *Geochimica et Cosmochimica Acta*, **51**,1939-1949.

Środoń J & Paszkowski M (2011) Role of clays in the diagenetic history of nitrogen and boron in the Carboniferous of Donbas (Ukraine). *Clay Minerals*, **46**,561–582.

Tassi F, Bonini M, Montegrossi G, Capecchiacci F, Capaccioni B & Vaselli O (2012) Origin of light hydrocarbons in gases from mud volcanoes and CH_4-rich emissions. *Chemical Geology*, **294-295**,113-126.

Tonarini S, Pennisi M & Gonfiantini R (2009) Boron isotope determinations in waters and other geological materials: Analytical techniques and intercalibration of measurements. *Isotopes in Environmental and Health Studies*, **45**,169-183.

Toran LE & Saunders JA (1999) Modeling alternative paths of chemical evolution of Na-HCO3-type groundwater near Oak Ridge, Tennessee, USA. *Hydrogeology Journal*, **7**,355-364.

Toscani L, Venturelli G & Boschetti T (2001) Sulphide-bearing waters in Northern Apennines, Italy: general features and water-rock interaction. *Aquatic Geochemistry*, **7**,195–216.

Veggiani A (1964) Le acque minerali del territorio di Bertinoro. *Studi Romagnoli*, **15**,143-164.

Vengosh A, de Lange GJ & Starinsky A (1998a) Boron isotope and geochemical evidence for the origin of Urania and Bannock brines at the eastern Mediterranean: Effect of water-rock interactions. *Geochimica et Cosmochimica Acta*,, **62**,3221–3228.

Vengosh A, Kolodny Y & Spivack AJ (1998b) Ground-water pollution determined by boron isotope systematics. In: *Applications of Isotopic Techniques to Investigate Ground-Water Pollution* Vienna (Austria), IAEA, IAEA-TECDOC-1046, 17-37.

Vengosh A, Gieskes J & Mahn C (2000) New evidence for the origin of hypersaline pore fluids in the Mediterranean basin. *Chemical Geology*, **163**,287–298.

Vengosh A, Starinsky A, Kolodny Y & Chivas AR (1991) Boron isotope geochemistry as a tracer for the evolution of brines and associated hot springs from the Dead Sea, Israel. *Geochimica et Cosmochimica Acta*, **55**,1689-1695.

Vengosh A, Starinsky A, Kolodny Y, Chivas AR & Raab M (1992) Boron isotope variations during fractional evaporation of sea water: New constraints on the marine vs. nonmarine debate. *Geology*, **20**,799-802.

Venturelli G, Boschetti T & Duchi V (2003) Na-carbonate waters of extreme composition: possible origin and evolution. *Geochemical Journal*, **37**,351–366.

Vinson DS, McIntosh JC, Dwyer GS, Warner NR & Vengosh A (2013) Boron desorption and boron isotopes in sodium bicarbonate coalbed methane waters. In: *125th Anniversary Annual Meeting & Exposition* Denver, Colorado, USA, The Geological Society of America, **45**, 758.

Williams LB & Hervig RL (2002) Exploring intra-crystalline B-isotope variations in mixed-layer illite-smectite. *American Mineralogist*, **87**,1564–1570.

Williams LB, Hervig RL, Wieser ME & Hutcheon I (2001a) The influence of organic matter on the boron isotope geochemistry of the gulf coast sedimentary basin, USA. *Chemical Geology*, **174**,445–461.

Williams LB, Hervig RL, Holloway JR & Hutcheon I (2001b) Boron isotope geochemistry during diagenesis. Part I. Experimental determination of fractionation during illitization of smectite. *Geochimica et Cosmochimica Acta*, **65**, 1769–1782.

Williams LB, Hervig RL & Hutcheon I (2001c) Boron isotope geochemistry during diagenesis. Part II. Applications to organic-rich sediments. *Geochimica et Cosmochimica Acta*, **65**,1783–1794.

Williams LB, Turner A & Hervig RL (2007) Intracrystalline boron isotope partitioning in illite-smectite: testing the geothermometer. *American Mineralogist*, **92**,1958–1965.

Wolery TW & Jarek RL (2003) EQ3/6, version 8.0 - software user's manual. In: Albuquerque, New Mexico, Civilian radioactive waste management system, Management & Operating Contractor, Sandia National Laboratories.

You CF, Spivack AJ, Gieskes JM, Martin JB & Davisson ML (1996) Boron contents and isotopic compositions in pore waters: a new approach to determine temperature induced artifacts geochemical implications. *Marine Geology*, **129**,351-361.

You CF, Spivack AJ, Smith JH & Gieskes JM (1993) Mobilization of boron in convergent margins: Implications for the boron geochemical cycle. *Geology*, **21**,207-210.

Zeebe RE (2005) Stable boron isotope fractionation between dissolved $B(OH)_3$ and $B(OH)_4^-$. *Geochimica et Cosmochimica Acta*, **2005**,2753–2766.

This is a preprint. Final version is subject to change. Cite as Authors (Year) Title. Geofluids, in press.
DOI: 10.1111/gfl.12124

Tab.1

Sample code	Locality	Sampling date	Lat-N	Long-E	Temp.	Cond.	Eh	pH	TDS	density	NH_4	H_2S	S-tot	T-Alk	Cl	Ca	Mg	Na	K	Sr	Br	SiO_2	B	B	$\delta^{18}O(H_2O)$	$\delta^{2}H(H_2O)$	$\delta^{11}B$
		dd.mm.yy			T °C	mS/cm 20°C	mV		g/l	kg/l	mg/l	mg/l	mg/l	mg/l	mg/l	mg/l	mg/l	mg/l	mg/l	mg/l	mg/l	mg/l	mg/l	mg/kg	‰ vs. V-SMOW	‰ vs. V-SMOW	‰ vs. SRM951
fresh Na-carbonate (Na-CAR)																											
F3	Roccaferrara	04.04.12	44°29'01.9"	10°02'18.5"	9.6	0.8	63	9.55	0.46	1.000	<	1.4	2	514	11.1	1.20	1.09	175	0.61	0.298	0.012	9.9	0.770	0.770	-9.24	-62.0	19.5
F6	Monti Bedonia	16.05.12	44°31'34.9"	09°38'35.8"	11.8	0.6	-19	9.31	0.33	1.000	0.75	0.44	<	361	4.9	1.63	0.89	130	1.11	0.286	0.013	9.9	0.587	0.587	-8.66	-55.3	6.1
F8	Vezzolo	08.05.12	44°27'22.9"	10°23'24.1"	11.7	1.25	-61	9.30	0.66	1.000	1.8	3.6	6	701	22.0	1.07	0.88	253	1.16	0.201	0.201	11.5	1.60	1.60	-9.81	-67.3	15.6
F10	Maiola	08.05.12	44°29'02"	10°24'28"	11.7	1.70	-30	9.26	0.88	1.000	0.51	3.6	2	716	148	1.38	0.92	345	1.25	0.289	1.02	13.5	3.91	3.91	-9.28	-68.4	23.8
F13	Varano Melegari	16:05:12	44°41'35"	9°59'45"	13.6	1.07	-53	8.74	0.61	1.000	0.36	1.0	17	584	10.6	3.07	3.58	234	0.99	0.199	0.057	15.3	1.43	1.43	-9.16	-62.2	27.2
brackish Na-chloride (Na-CHL)																											
MI	Miano	04.04.12	44°29'19"	10°05'43.5"	39.4	6.9	-	8.10	4.0	1.003	2.8	0.1	-	315	2284	36.3	6.00	1446	19	6.79	-	23.9	11.2	11.2	-8.64	-58.3	14.0
SAL	Salvarola	25:10:06	44°31'04.8"	10°46'05.4"	15.3	25.0	227	8.37	16	1.007	1.9	13	3	2079	8490	4.70	12.6	5950	18	4.04	101	11.4	105	104	3.66	-15.2	18.9
saline Ca-chloride (Ca-CHL)																											
CSP	Castelsanpietro	05:10:06	44°23'13.1"	11°35'19"	20.3	50.0	92	7.70	33	1.019	54	-	0.90	430	20206	311	606	11000	185	16.4	158	9.2	7.51	7.37	0.01	0.6	26.6
FRA	Fratta	24:05:07	44°08'29.7"	12°06'01"	12.8	92.8	93	6.70	75	1.050	88	11	0.85	123	47394	1780	1080	23500	219	279	198	9.1	10.7	10.2	-1.70	-16.5	22.9
brine Ca-chloride (Ca-CHL)																											
MON	Monticelli	10:11:06	44°43'39.9"	10°23'42.9"	15.8	141	130	6.83	116	1.080	82	-	0.6	57	73015	5670	2470	34500	234	318	480	7.2	17.8	16.5	-0.74	-11.6	37.9
TOL	Tolentino	13:11:07	43°12'51.9"	13°15'29"	13.7	133	270	6.23	118	1.094	50	2.4	5.5	87	74374	5752	2301	35732	164	553	362	9.6	8.15	7.45	0.48	-7.4	35.1
SM	Salsomaggiore	07:11:07	44°48'17.4"	9°58'12.4"	16.9	175	112	6.98	152	1.103	211	-	27	187	96108	4270	1210	49700	274	343	360	5.5	358	325	11.37	-16.0	13.4

TDS (calculated total dissolved solids) = 0.5*Alkalinity(as HCO_3)+Ca+Mg+Na+K+Cl+SO_4+(2.82*H_2S)+(1.02*SiO_2) (Eaton et al. 1996)
density = measured when TDS > 1, calculated with PHREEQCI when TDS < 1. However, density = 1.000 at the third decimal aproximation when TDS < 1
NH_4 = sum of NH_4^+ and $NH_3°$
H_2S = sum of $H_2S°$, HS^-, S^{2-}
S-tot = total sulfur measured by ICP-AES
T-Alk = total alkalinity as HCO_3
< = below detection limit
- = not measured

Fig 1

Fig 2

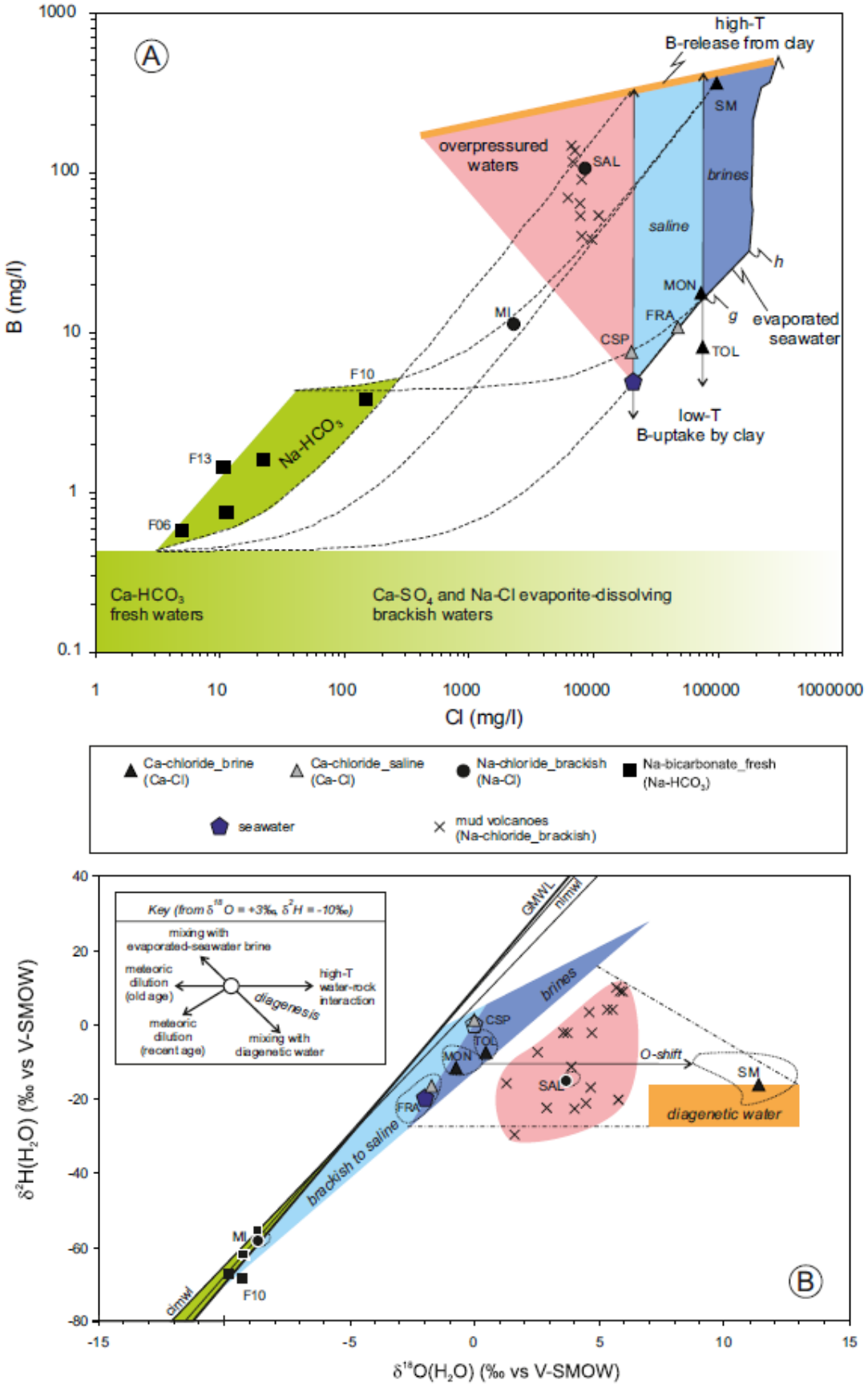

Fig. 3

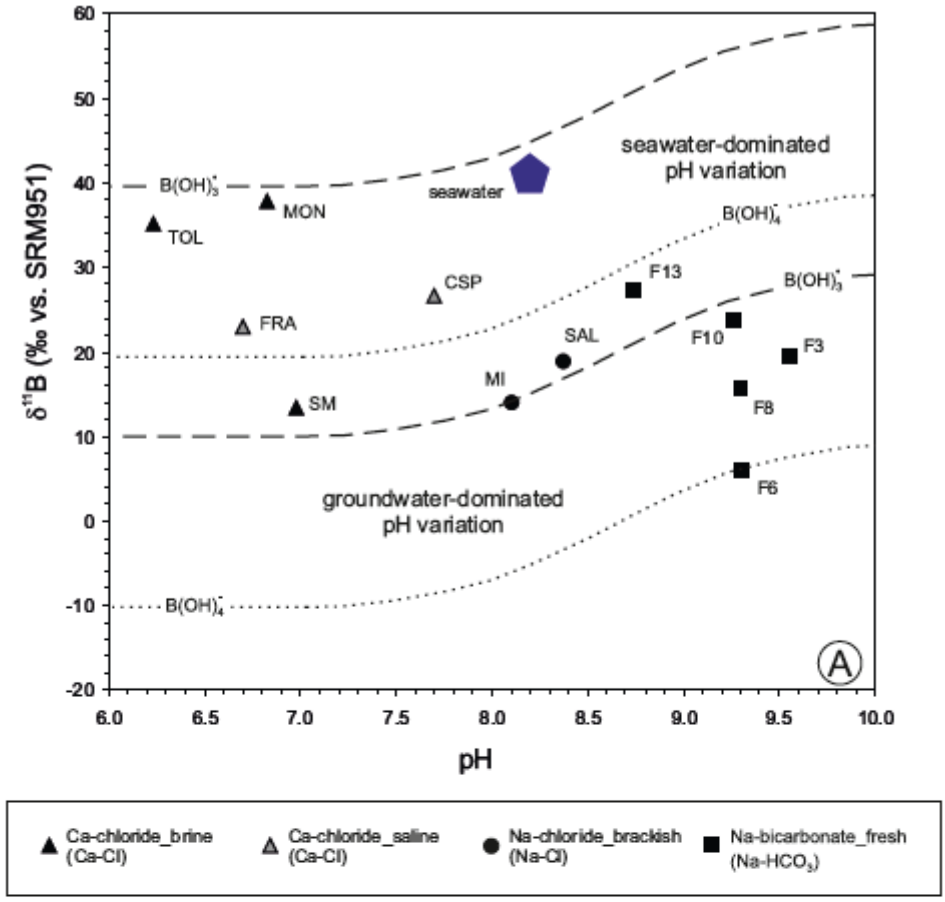

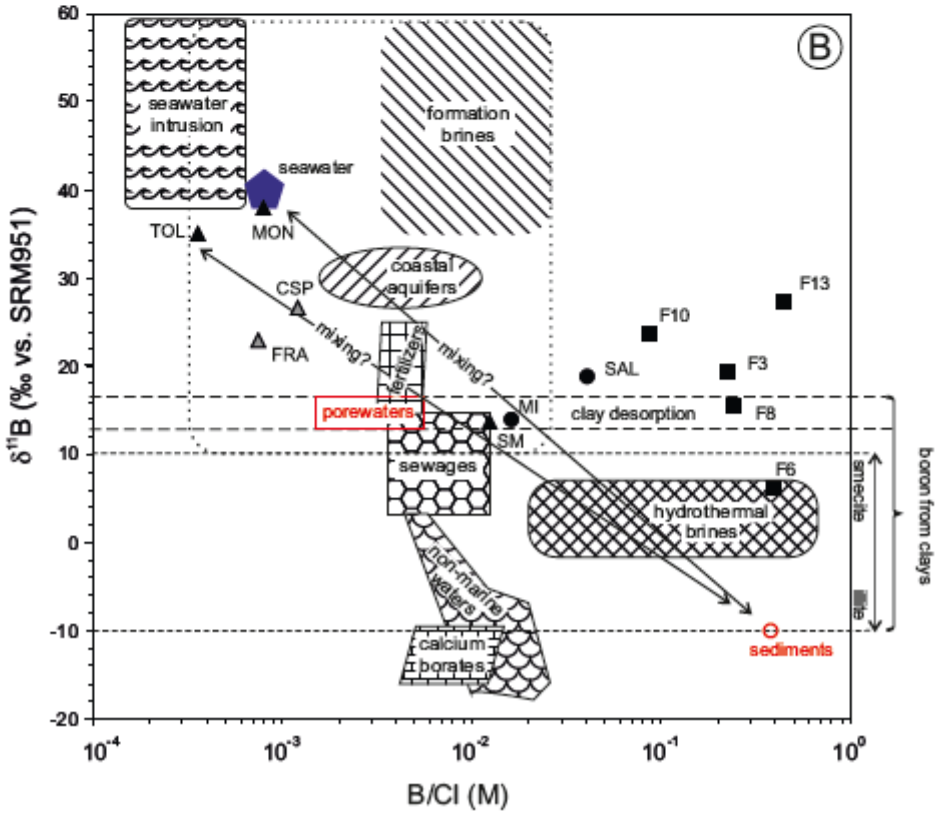

Fig. 4

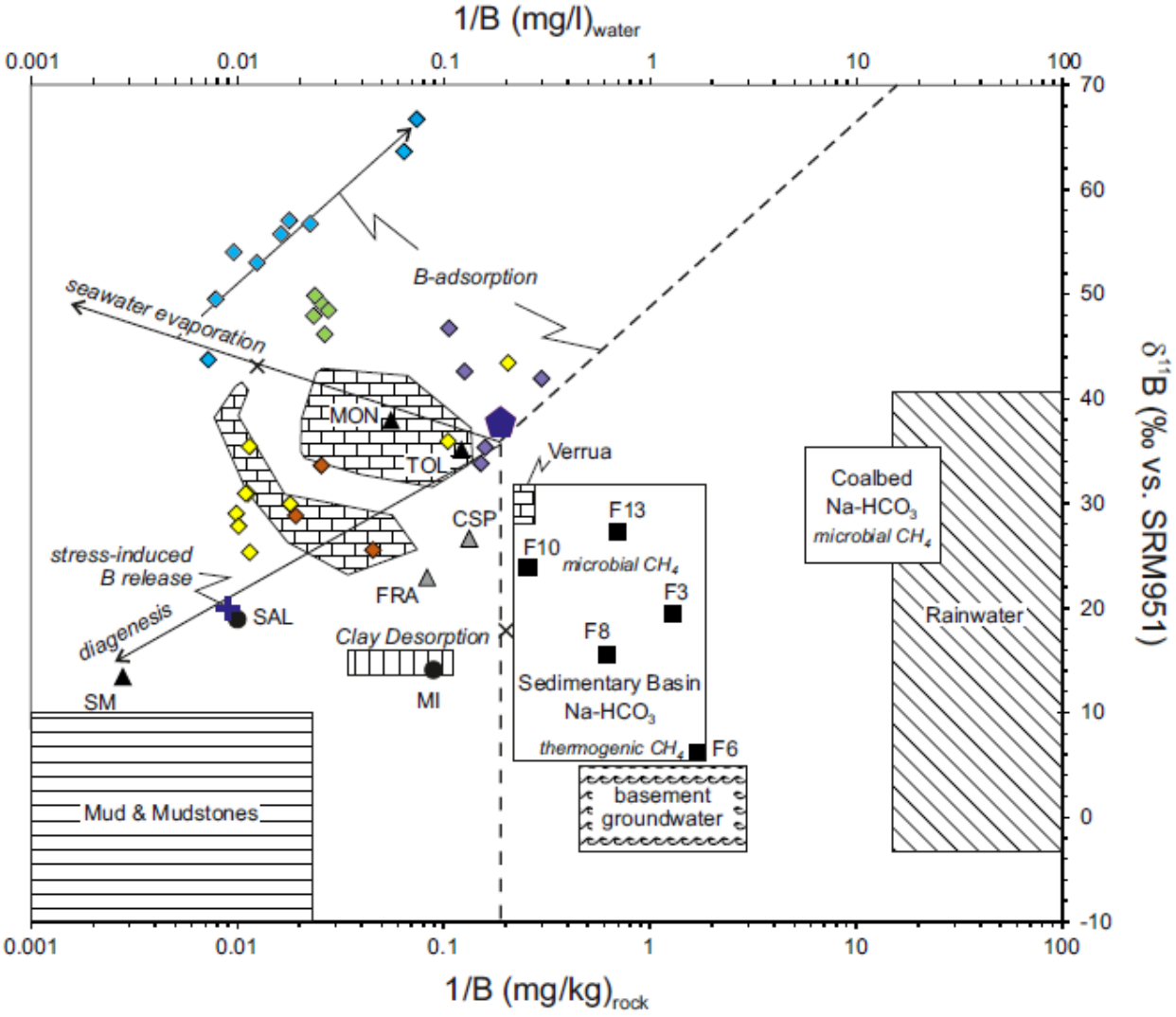

Literature	This study
Mediterranean Sea	Ca-chloride_brine (Ca-Cl)
Porewaters	
DSDP site 374	Ca-chloride_saline (Ca-Cl)
DSDP site 372	
Bannock	Na-chloride_brackish (Na-Cl)
Urania	
Mud Volcanoes	Na-bicarbonate_fresh ($Na-HCO_3$)
Napoli	
Milano-Napoli-Verrua (inferred by aut. carbonates)	
NAF	

Fig. 5

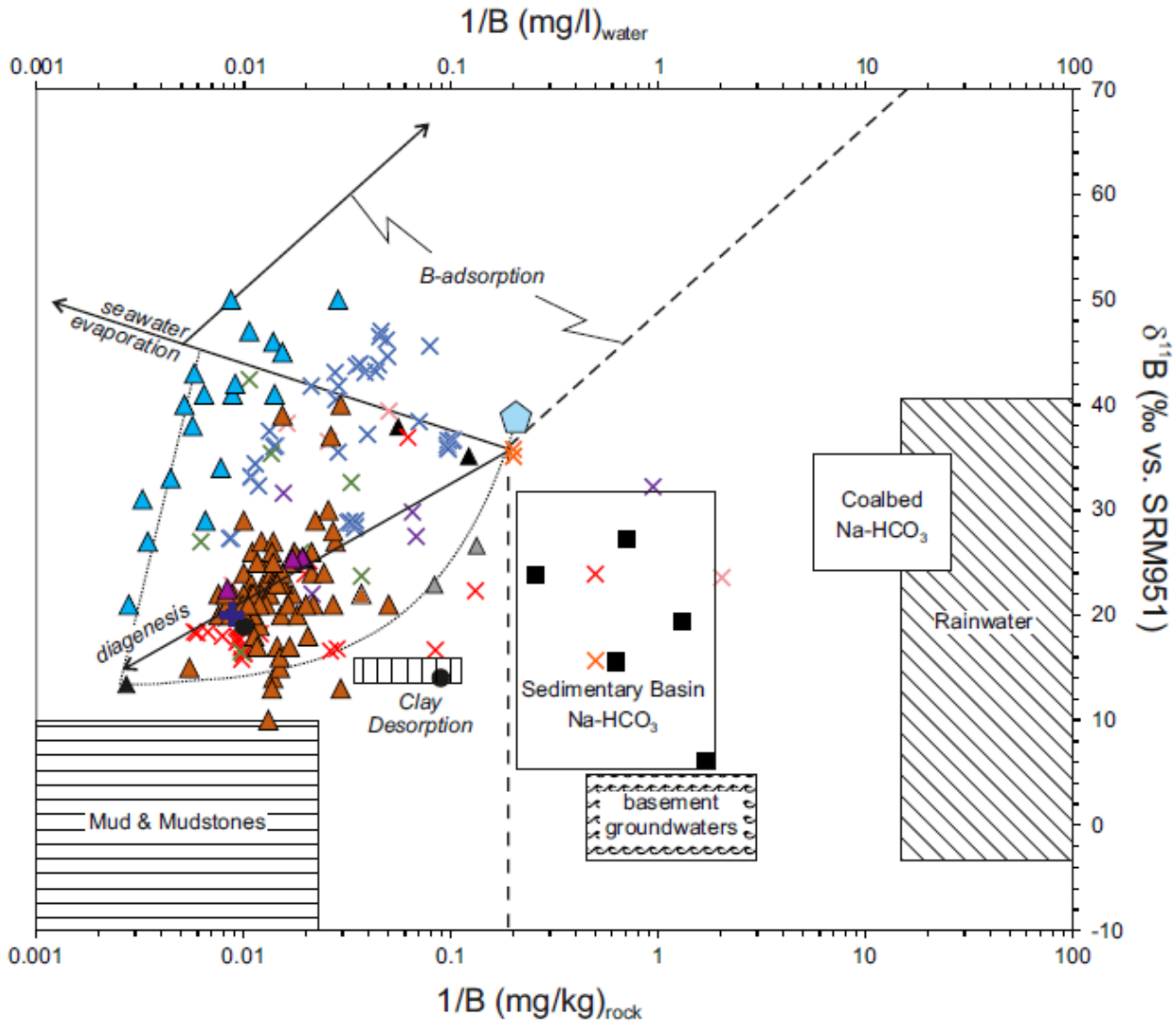

Literature	This study
Mean Ocean Water	Ca-chloride_brine (Ca-Cl)
Formation brines	Ca-chloride_saline (Ca-Cl)
Gulf Coast (carb. aq.)	Na-chloride_brackish (Na-Cl)
Gulf Coast (silicocl. aq.)	Na-bicarbonate_fresh ($Na-HCO_3$)
France	
Mud Volcanoes	
Taiwan (marine)	
Taiwan (terrestrial)	
Taman (Caucasus)	
ChandraGup (India)	
Tarim (China)	
Georgia (Caucasus)	

This is a preprint. Final version is subject to change. Cite as Authors (Year) Title. Geofluids, in press.
DOI: 10.1111/gfl.12124

Fig. 6

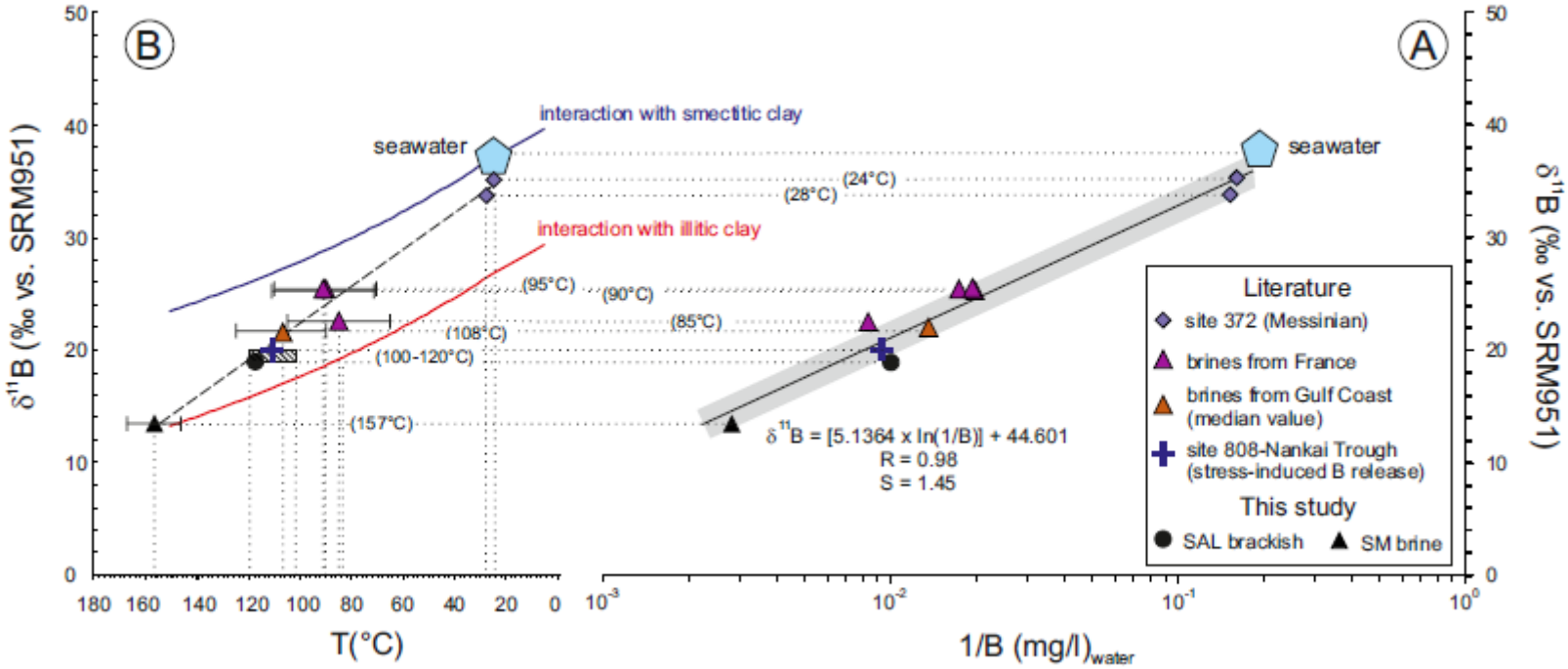

This is a preprint. Final version is subject to change. Cite as Authors (Year) Title. Geofluids, in press.
DOI: 10.1111/gfl.12124

Appendix 1

Boron speciation calculation*

fresh Na-carbonate (NaCAR)

SIT	B tot	boric acid	borates	boric acid	borates	Btot check	Debye-Hückel	B tot	boric	borates	boric	borates	Btot check	**Average**	**boric**	**borates**	**References**
	mol/kg H2O	mol/kg H2O	mol/kg H2O	%	%	%		mol/kg H2O	mol/kg H2O	mol/kg H2O	%	%	%		**%**	**%**	
F3	7.13E-05	2.18E-05	4.95E-05	31	69	100	**F3**	7.13E-05	2.85E-05	4.28E-05	40	60	100	**F3**	**35**	**65**	this work
F6	5.43E-05	2.38E-05	3.06E-05	44	56	100	**F6**	5.43E-05	2.87E-05	2.57E-05	53	47	100	**F6**	**48**	**52**	this work
F8	1.48E-04	6.45E-05	8.37E-05	44	56	100	**F8**	1.48E-04	7.77E-05	7.04E-05	52	48	100	**F8**	**48**	**52**	this work
F10	3.62E-04	1.65E-04	1.98E-04	45	55	100	**F10**	3.62E-04	1.96E-04	1.66E-04	54	46	100	**F10**	**50**	**50**	this work
F13	1.32E-04	9.76E-05	3.48E-05	74	26	100	**F13**	1.32E-04	1.05E-04	2.75E-05	79	21	100	**F13**	**76**	**24**	this work
F13/98	1.73E-04	9.19E-05	8.12E-05	53	47	100	**F13/98**	1.73E-04	9.58E-05	7.73E-05	55	45	100	**F13/98**	**54**	**46**	Toscani et al. 2001

brackish Na-chloride (NaCHL)

SIT	B tot	boric acid	borates	boric acid	borates	Btot check	Debye-Hückel	B tot	boric	borates	boric	borates	Btot check	**Average**	**boric**	**borates**	
	mol/kg H2O	mol/kg H2O	mol/kg H2O	%	%	%		mol/kg H2O	mol/kg H2O	mol/kg H2O	%	%	%		**%**	**%**	
MI	1.04E-03	9.22E-04	1.15E-04	89	11	100	**MI**	1.04E-03	9.24E-04	1.14E-04	89	11	100	**MI**	**89**	**11**	Boschetti et al. 2011
SAL	9.81E-03	8.26E-03	1.55E-03	84	16	100	**SAL**	9.81E-03	8.25E-03	1.56E-03	84	16	100	**SAL**	**84**	**16**	Boschetti et al. 2011

saline Ca-chloride (Ca-CHL)

B-DOT	B tot	boric acid	borates	boric acid	borates	Btot check	Pitzer	B tot	boric acid	borates	boric acid	borates	Btot check	**Average**	**boric**	**borates**	
	mol/kg H2O	mol/kg H2O	mol/kg H2O	%	%	%		mol/kg H2O	mol/kg H2O	mol/kg H2O	%	%	%		**%**	**%**	
CSP	8.10E-04	7.49E-04	6.13E-05	92	8	100	**CSP**	7.04E-04	6.56E-04	4.82E-05	93	7	100	**CSP**	**93**	**7**	Boschetti et al. 2011
FRA	1.01E-03	1.00E-03	1.25E-05	99	1	100	**FRA**	1.01E-03	1.00E-03	1.30E-05	99	1	100	**FRA**	**99**	**1**	Boschetti et al. 2011

brine Ca-chloride (Ca-CHL)

B-DOT	B tot	boric acid	borates	boric acid	borates	Btot check	Pitzer	B tot	boric acid	borates	boric acid	borates	Btot check	**Average**	**boric**	**borates**	
	mol/kg H2O	mol/kg H2O	mol/kg H2O	%	%	%		mol/kg H2O	mol/kg H2O	mol/kg H2O	%	%	%		**%**	**%**	
MONT	1.71E-03	1.66E-03	5.16E-05	97	3	100	**MONT**	1.71E-03	1.65E-03	6.30E-05	96	4	100	**MONT**	**97**	**3**	Boschetti et al. 2011
TOL	7.73E-04	7.67E-04	5.80E-06	99	1	100	**TOL**	7.73E-04	7.66E-04	7.30E-06	99	1	100	**TOL**	**99**	**1**	Boschetti et al. 2011
SM	1.35E-02	1.30E-02	4.83E-04	96	4	100	**SM**	1.35E-02	1.28E-02	7.00E-04	95	5	100	**SM**	**96**	**4**	Boschetti et al. 2011
SM[+]	1.35E-02	1.30E-02	5.68E-04	96	4	100	**SM***	1.35E-02	1.30E-02	5.60E-04	96	4	100	**SM***	**96**	**4**	Boschetti et al. 2011

[+]T = 150°C, P = 650 bar

*Activity calculation method	software	database
Debye-Hückel	PHREEQCI	llnl.dat
SIT	PHREEQCI	sit.dat
B-DOT	EQ3/6	data0.cmp
Pitzer	PHREEQCI	pitzer.dat

This is a preprint. Final version is subject to change. Cite as Authors (Year) Title. Geofluids, in press.
DOI: 10.1111/gfl.12124

Appendix 2a

Data used for the calculation of the diagenetic equation (Fig.6A)

Sample	**Temperature**	**B**	**1/B**	**$\delta^{11}B$**	**Samples name in the reference**	**References (T, B, $\delta^{11}B$)**
Sample Name in Fig. 5	°C	mg/l	mg/l	‰ vs. SRM951		
site 372	24	6.27	0.159	35.3	DSDP 372, 3-2 (depth: 148 m)	Erickson and Von Herzen 2007; Vengosh et al. 2000
	28	6.59	0.152	33.8	DSDP 372, 9-3 (depth: 203 m)	Erickson and Von Herzen 2007; Vengosh et al. 2000
brines from France	90	51	0.0196	25.3	Chaunoy72	Millot et al. 2011
	90	52	0.0192	25.5	Chaunoy73	Millot et al. 2011
	85	120	0.00833	22.5	La Torche	Millot et al. 2011
	90	50	0.0200	25.4	Champotran	Millot et al. 2011
SAL	110	105	0.00952	18.9	Salvarola	this study; Boschetti et al. 2011; Tassi et al. 2012
SM	157	358	0.00279	13.4	Salsomaggiore	this study; Boschetti 2013; Boschetti et al. 2011
site 808-Nankai Trough	110	108	0.0092498	20.0	site 808-Nankai Trough	Moore et al. 2005; You et al. 1996
brines from Gulf Coast (median value)	108	74	0.0135	22.0	*median values of 78 brine samples*	Land 1995; Land and MacPherson 1992; Williams et al. 2001c

This is a preprint. Final version is subject to change. Cite as Authors (Year) Title. Geofluids, in press.
DOI: 10.1111/gfl.12124

Appendix 2b

Statistical analysis of the δ^{11}B-T linear regression

	Temperature	δ^{11}B
	°C	‰ vs. SRM951
site 372	24	35.3
	28	33.8
brines from France	90	25.3
	90	25.5
	85	22.5
	90	25.4
SAL	110	18.9
SM	157	13.4
site 808-Nankai Trough	110	20.0
brines from Gulf Coast (median value)	108	22.0

Linear Regression Statistic	
R multiple	0.979
R square	0.958
R corrected square	0.952
Standard Error	1.435
Values	10

Variance analysis

	degrees of freedom	*SQ*	*MQ*	*F*	*F significativity*
Regressione	1	373.3276332	373.3276	181.211977	8.89004E-07
Residuo	8	16.48136682	2.060171		
Totale	9	389.809			

	Coefficients	*Standar Errors*	*Stat t*	*Significativity*	*<95%*	*<95%*
Y	38.87314307	1.180049036	32.94197	7.86569E-10	36.15194512	41.59434103
X	-0.164366585	0.012210124	-13.4615	8.89004E-07	-0.192523182	-0.136209988